Journal of Marine Science and Application (2026) 25: 1318-1331
https://doi.org/10.1007/s11804-026-00863-0

RESEARCH ARTICLE

CFD–DEM Simulation of Erosion Degradation Mechanisms in Deep-Sea Mining Pipelines

Hao Zhang[1,2], Wentao Hu[2], Fengwei Xu[2], Peng Gong[2] and Ziyue Han[3]

Received: 17 March 2025 / Accepted: 07 November 2025
© Harbin Engineering University and Springer-Verlag GmbH Germany, part of Springer Nature 2026

Abstract

As terrestrial mineral resources continue to diminish, the global focus has significantly shifted toward deep-sea mining, driven by the escalating demand for critical minerals such as lithium, nickel, and cobalt. Among various extraction methods, the pipe lifting technique has gained prominence owing to its substantial commercial viability. Nevertheless, this method faces significant operational challenges, including intricate flow dynamics, pipe wall erosions, and blockages caused by the continuous transport of particulate matter. This study investigates the influence of mineral particle size, the slurry velocity, volume fraction, and shear modulus on pipeline erosion. To enhance the precision of erosion prediction, a solid-liquid coupling optimization model was developed utilizing the Gaussian volume distribution method. Orthogonal experiments and single-factor analyses revealed that the slurry velocity and mineral particle size predominantly influence the erosion rate. The findings of this study elucidate the underlying mechanisms of pipeline erosion in deep-sea mining operations and offer crucial data for the advancement and design of deep-sea transportation systems.

Keywords Deep-sea mining pipeline; Erosion prediction; Liquid–solid flow; Coarse mineral particles; High volume fraction slurry

1 Introduction

The escalating depletion of terrestrial mineral resources has propelled deep-sea mineral resource development technologies to the forefront of global attention, driven by the surging demand for critical minerals such as lithium, nickel, and cobalt. Among the various extraction methods, the pipe lifting technique has emerged as the most commercially viable approach for deep-sea mining. However, deep-sea mining pipelines, a critical component of the transportation system, face significant operational challenges. These include complex internal flow dynamics (Liu et al., 2023), the inhospitable seabed environment, and the continuous transport of mineral particles, all of which contribute to pipe wall erosion and flow path blockages. Deep-sea mining technology has advanced significantly in recent years. Cai et al. (2020) developed a bionic grouser structure based on bionics principles, which significantly improved the walking stability and collection efficiency of mining vehicles by optimizing geometric parameters. Liu et al. (2020) innovatively proposed a pipeline-walking mining robot that uses drive components to control the walking mechanism of lifting piles and has demonstrated excellent operational stability on manganese nodule geological layers. However, these innovative technologies targeting mining vehicles have not yet effectively addressed the complex erosion problems faced by deep-sea mining pipelines. To overcome these challenges, the erosion mechanisms of two-phase flow within pipelines must be comprehensively investigated (Kleis and Kulu 2007). Analyzing parameter variations under diverse conditions is essential for understanding failure modes. Furthermore, studying the erosion behavior of coarse mineral particles during deep-sea mining provides valuable insights that are

Article Highlights

- This study establishes an enhanced solid–liquid coupling erosion prediction model that incorporates a Gaussian volume distribution method to more accurately represent the motion and collision behavior of large mineral particles in deep-sea mining pipelines.
- A CFD–DEM numerical framework is developed to overcome the limitations of conventional DPM- or DEM-based approaches, enabling the simultaneous consideration of particle–fluid and particle–particle interactions under high particle volume fractions typical of deep-sea mineral transport.
- The proposed model systematically quantifies the effects of slurry velocity, particle size, particle volume fraction, and shear modulus on erosion progression, thereby providing a comprehensive understanding of erosion characteristics under realistic operational conditions.

✉ Hao Zhang
zhanghaocoolcool@163.com

[1] School of Mechanical Science and Engineering, Huazhong University of Science and Technology, Wuhan 430074, China

[2] China Ship Scientific Research Center, Wuxi 214082, China

[3] School of Resources Engineering, Xi'an University of Architecture and Technology, Xi'an 710055, China

instrumental in developing and designing efficient deep-sea mining transportation systems.

Erosion issues in deep-sea mining pipelines, particularly conveyance hoses, have been extensively studied using full-size or scaled physical models. Helgaker et al. (2017) conducted sand erosion experiments on a 9.75 inch diameter flexible pipeline with a 2.5 m bend radius to investigate the erosion effects of sand and proppant particles at velocities ranging from 30 to 47 m/s. Similarly, Parenteau (2012) introduced an innovative approach to mitigate particle erosion in pumps during recirculation. Using a large-scale experimental platform, they tested pressure losses and erosion rates under conditions involving particle concentrations of 10%–45%, flow rates of 2.5–5.5 m/s, an 8 inch flexible pipe, and equivalent rock particles, relevant to deep-water mining projects. Rongau and Viale (2017) developed a flexible riser for deep-sea mining featuring an abrasion-resistant inner layer to withstand slurry wear and an outer layer to bear mechanical loads. They conducted large-scale tests to compare the wear properties of rubber, polyethylene, and stainless steel, aiming to select the most effective abrasion-resistant material. Takano et al. (2022) evaluated pipe wear caused by slurry flow through full-scale experiments, concluding that SUS304 stainless steel demonstrated superior wear resistance compared with ultra-high molecular weight polyethylene. Their findings indicated that vertical pipes experienced uniform wall thickness reduction, whereas horizontal and inclined pipes exhibited erosion primarily concentrated along the bottom inner wall of the pipe.

The Euler–Lagrange coupled model has become the predominant method for particle tracking and erosion analysis. Yu et al. (2022) employed computational fluid dynamics (CFD) simulations to investigate erosion in unbonded flexible pipelines (UFPs) and introduced a simplified assessment methodology. Using three distinct erosion models to predict damage, they proposed improvements to geometric factors to enhance the accuracy of UFP carcass erosion predictions. Similarly, Zhang et al. (2019) developed a simplified model for predicting solid particle erosion in pipe bends by calculating particle trajectories based on momentum conservation and fluid drag mechanisms. Their findings were experimentally validated, providing insights into the model's applicability. Kannojiya et al. (2018) utilized numerical simulation to examine particle-induced erosion in pipe bends, incorporating solid–liquid, solid–solid, and solid–wall interactions to assess erosion rates under varying particle sizes, concentrations, and slurry velocities. Lain and Sommerfeld (2019) adopted the Euler–Lagrange approach, integrating turbulence models and two-way coupling to estimate particle erosion in pipe bends. Their analysis highlighted the influence of various transport phenomena on pipeline erosion, revealing that particle–particle collisions significantly reduced erosion depth. Agrawal et al. (2019) advanced this research by incorporating dynamically changing pipe geometry into CFD models through dynamic deformation meshes, enabling real-time adjustments to pipe walls and thereby improving erosion prediction accuracy. Kannojiya et al. (2016) explored erosion in slurry pipelines using the Euler–Lagrange method to simulate multiphase flows. They applied the stochastic model proposed by Sommerfeld (2003) to account for pipe wall roughness and examined the effects of fluid velocity, particle size, and concentration on erosion behavior. Peng and Gao (2016) addressed gas–solid flow challenges using a two-way coupled Euler–Lagrange approach, integrating the Det Norske Veritas erosion model with the Forder particle rebound model. Their study analyzed erosion distribution and particle trajectories under various conditions, identifying two types of erosion marks and three collision patterns. They also proposed an equation to predict the locations of maximum erosion. Wang et al. (2017) investigated the effects of elbow orientation and particle characteristics on erosion, as well as the relationship between secondary flow and particle trajectories. Their results showed that erosion predominantly occurred near the elbow outlet, whereas sidewalls remained unaffected when the secondary flow was weak.

The primary solid–liquid two-phase flow models used in numerical calculations include the discrete phase model (DPM), discrete element method (DEM), and coupled DPM–DEM models (Chen et al., 2022). The DPM is typically applied to scenarios with particle volume fractions below 10%, as it does not account for interparticle interactions (Zahari et al., 2018). Conversely, the DEM primarily focuses on simulating particle interactions but neglects solid–liquid interactions. The DPM model mainly focuses on the interaction between particles and fluid, ignoring the interaction between particles. Although the CFD–DEM model is more comprehensive than the individual DPM and DEM models, it requires fluid meshes at least three times the particle size, limiting its practicality (Sande and Ray, 2014). These traditional models are inadequate for studying erosion in deep-sea mining pipelines owing to their inherent limitations.

In deep-sea mining, particle diameters typically range from 5 to 30 mm, and the mineral volume fraction can reach up to 30%. During mineral transport, the interactions among mineral particles and between particles and fluids are significant and cannot be overlooked. This complexity makes it difficult for existing research tools to accurately capture the erosion characteristics of pipelines under deep-sea mining conditions, particularly when dealing with large mineral particles. Consequently, several critical issues remain unresolved, including the need for more robust models that can effectively simulate the intricate dynamics of solid–liquid interactions and erosion mechanisms in such environments. Addressing these challenges is essential for advanc-

ing the design and optimization of deep-sea mining transportation systems.

• Existing solid–liquid coupling models (e.g., DPM and DEM) are primarily designed for small particles (<10 mm) and fail to accurately capture the motion, collisions, and erosion behavior of large mineral particles in deep-sea mining pipelines. Considering the high volume fraction (up to 30%) and complex interactions between particles and fluid in deep-sea mining, current models remain inadequate for predicting erosion locations, depths, and rates. Therefore, a solid–liquid coupling model specifically tailored for large mineral particles must be developed to better simulate erosion mechanisms in deep-sea mining environments.

• Recent research has predominantly focused on the mechanical properties, spatial characteristics, and vibrations of pipelines, with limited attention given to erosion characteristics. Although some studies have investigated erosion and pressure drop in deep-sea mining pipelines through physical experiments, the inherent limitations of these experiments restrict their ability to comprehensively analyze the influence of factors such as pipeline curvature, mineral particle size, and mineral concentration on erosion. Therefore, a systematic investigation combining numerical simulations and experimental approaches is essential to understand the effects of these factors on pipeline erosion and to provide theoretical support for the design and optimization of deep-sea mining transportation systems.

The aim of this study is to investigate the erosion behavior of mineral particles with diameters ranging from 5 to 30 mm. A numerical model of an arched pipeline, along with an erosion model, was developed based on the actual spatial configuration and operational conditions of deep-sea mining pipelines. A coupled computational approach (CFD–DEM) is employed to solve the continuous and discrete phases within the Euler–Lagrange framework, enabling a comprehensive analysis of system dynamics. Furthermore, orthogonal experimental design and single-factor influence analysis are conducted to evaluate the effects of key parameters, including slurry flow rate, mineral particle size, and volume fraction, on pipeline erosion.

The rest of the paper is structured as follows: Section 2 introduces the mathematical model of deep-sea mining pipelines, including fluid control equations, particle control equations, and the erosion model. Section 3 presents the parameters of deep-sea mining pipes, such as material and geometric dimensions, as well as mesh division methods and boundary condition settings. Sections 4 and 5 present the orthogonal experimental analysis and single-factor influence analysis of the results, respectively, to explore the importance and sensitivity of various influencing factors and analyze the erosion characteristics of deep-sea mining transport pipes under different conditions. Finally, Section 6 concludes the paper.

2 Mathematical model

2.1 Fluid control equations

The fluid is treated as a continuous phase, with its behavior governed by equations derived from Navier–Stokes (N–S) equations. The key assumption of this model is the fluid continuity assumption, which neglects the microscopic gaps between fluid molecules and treats the fluid as a continuum. This assumption enables us to effectively describe the macroscopic characteristics of solid–liquid two-phase flow in deep-sea mining pipelines, ensuring that the simulation results accurately reflect flow behavior in actual engineering. A fluid disturbance term is introduced into the momentum equation to represent the influence of particles on fluid motion during flow. The governing equation for fluid motion within the pipeline is as follows:

$$\left\{\begin{array}{l} \dfrac{\partial}{\partial t}\left(\varepsilon_f \rho_f\right) + \nabla \cdot \left(\varepsilon_f \rho_f u_f\right) = 0 \\ \dfrac{\partial}{\partial t}\left(\varepsilon_f \rho_f u_f\right) + \nabla \cdot \left(\varepsilon_f \rho_f u_f u_f\right) = -\varepsilon_f \nabla p_f + \nabla\left(\varepsilon_f R_f\right) + \\ \qquad \varepsilon_f \rho_f g + f_{\mathrm{sf}} \end{array}\right\} \tag{1}$$

where ρ_f represents the fluid density; u_f is the fluid velocity; p_f is the fluid pressure; g is the gravitational acceleration; f_{sf} is the volumetric force exerted by particles on the fluid; R_f is the stress tensor, which includes both viscous and Reynolds stresses; ε_f is the fluid volume fraction, which can be calculated from the particle volume fraction.

For mineral particles, Gaussian weighting can be introduced to assign weights to each grid cell occupied by the minerals. The weight is determined by the distance between the grid center and the particle center, allowing for a better calculation of the volume occupied by the particles. The fluid volume fraction and Gaussian weighting are calculated as follows:

$$\left\{\begin{array}{l} \varepsilon_f = 1 - \dfrac{V_{\mathrm{particle}} \cdot G_{\mathrm{particle-VolumeWeight}}}{G_{\mathrm{total-cellWeight}} \cdot V_{\mathrm{cell}}} \\ G = \mathrm{e}^{-\left(\frac{a^d{}_{\mathrm{GaussCoeff}}}{\gamma \cdot a_{\mathrm{cuberatio}}}\right)^2} \end{array}\right\} \tag{2}$$

where V_{particle} is the volume of the particle; $V_{\mathrm{particle\text{-}VolumeWeight}}$ is the weight based on the distance between the particle and the current grid center, calculated using a Gaussian weighting function that decays with distance, giving closer particles a greater influence on the grid. $V_{\mathrm{total-cellWeight}}$ is the total weight calculated for all relevant grid cells, used for normalization to ensure that the volume fraction calculation accounts for the influence of particles on multiple cells. V_{cell} is the volume of the current grid cell. G is the Gaussian volume weight, representing the weighting factor of a particle on the grid cell it influences.

2.2 Particle control equations

In the particle control equations, an approach different from the traditional DPM is adopted. The traditional model usually assumes particles to be volume-less and shapeless mass points and neglects factors such as rotation. However, for large mineral particles in deep-sea mining, the rotational motion of particles must be considered. By establishing separate translational and rotational motion equations, the particle's dynamic behavior can be described more accurately, thereby improving the accuracy of simulation results.

$$\begin{cases} m_p \dfrac{\mathrm{d}u_p}{\mathrm{d}t} = m_p g + f_{\mathrm{fs}} + f_c \\ I_p \dfrac{\mathrm{d}\omega_p}{\mathrm{d}t} = M_{\mathrm{ct}} + M_{\mathrm{fs}} \end{cases} \tag{3}$$

where m_p is the mass of the particle; u_p is the particle velocity; f_{fs} is the force exerted by the fluid on the particle; f_c represents the contact force between particles, modeled using the Hertz–Mindlin no-slip contact theory; I_p is the moment of inertia of the particle; and ω_p is the angular velocity of the particle. M_{ct} is the contact torque between the particle and all other particles. M_{fs} is the torque exerted by the fluid on the particle. The force exerted by the fluid on the particle is expressed by the following equation (Loth and Dorgan, 2009):

$$f_{\mathrm{fs}} = f_d + f_l + f_p + f_{\mathrm{am}} \tag{4}$$

where f_d is the drag force, using the Schiller–Naumann drag model modified by Di Felice, which accurately characterizes the fluid resistance properties under high particle concentration conditions by introducing the void fraction function χ; f_l is the lift force, based on Saffman's lift theory, which quantifies the lateral lift effect on particles in a shear flow field; f_p is the pressure gradient force, reflecting the effect of the fluid pressure field on particles, with its magnitude proportional to the particle volume and local pressure gradient; f_{am} is the added mass force, accounting for the equivalent inertial force generated by the surrounding fluid driven by the accelerating motion of the particle.

2.3 Erosion model

The wear caused by erosion in pipelines is defined as the material loss from the pipe wall due to repeated collisions between discrete particles and the inner wall of the pipeline (Sommerfeld, 2003). When mineral particles flow along the inner surface of the pipeline, abrasive wear occurs. For this type of wear, the Oka erosion model (Oka et al., 2005) is used to calculate and analyze pipeline performance. This model considers the effects of particle size, velocity, and target material hardness on the erosion rate in the erosion prediction model. Wang et al. (2022) demonstrated that the Oka model is applicable to erosion simulations of deep-sea mining pipelines by comparing experimental data with simulation results. The formula is as follows:

$$E_R = 1.0 \times 10^{-9} \rho_w k F(\theta) (Hv)^{k_1} \left(\frac{V_p}{V'}\right)^{k_2} \left(\frac{d}{d'}\right)^{k_3} \tag{5}$$

$$F(\theta) = (\sin\theta)^{n_1} \left[1 + Hv(1 - \sin\theta)\right]^{n_2} \tag{6}$$

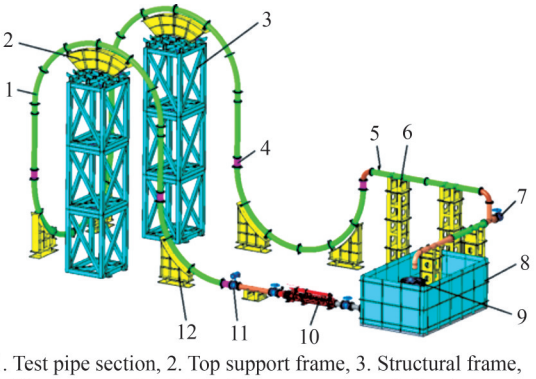
$$n = s \cdot Hv^q \tag{7}$$

where, E_R is the erosion rate; ρ_w is the density of the target material (kg/m³); Hv is the Vickers hardness of the target material (GPa); V_p and V' are the particle and reference velocities, respectively, (m/s); d and d' are the particle and reference diameters, respectively (μm); θ is the impact angle of the particle on the wall (rad); k, k_1, k_2, n_2, and n_2 are empirical parameters that depend on the material properties.

3 Computational model and parameters

3.1 Pipeline geometry model and mesh generation

The pipe material is an unbonded flexible hose (Rongau and Viale, 2017), which is customized by multi-layer metal and polymer materials for deep-sea mining, and its lining material is nylon 12.The pipe diameter (D) is 200 mm, the length of the vertical pipe section (L) is 2 m, and the bend radius (R) varies in the range of 1–3 m. The upper bend section of the experimental setup is selected as the research subject, as shown in Figure 1.



1. Test pipe section, 2. Top support frame, 3. Structural frame,
4. Flange expansion joints, 5. Pressure sensor, 6. Bracket,
7. Check valves, 8. Water tank, 9. Feeding device, 10. Slurry pump,
11. Flow regulating valve, and 12. Bottom support frame

Figure 1 Experimental setup

The slurry in the pipeline is treated as a continuous medium, with a flow velocity (V) of 2.5–4.5 m/s. The fluid enters from the left side and exits from the right side, and

the pipeline geometry (taking R = 1 m as an example) is shown in Figure 2. During the deep-sea mining process, it is not feasible for mechanical equipment to crush the collected ore to a uniform particle size; therefore, the average particle size is used as representation. The particle size distribution follows a normal distribution function. The particle size of polymetallic nodules (d) ranges from 5 to 30 mm (Parenteau et al., 2012). A normal distribution is used as the particle size distribution function, with average particle sizes of 8, 14, 20, and 26 mm selected. The mineral volume fraction (v) ranges from 5% to 20%.



Figure 2 U-shaped pipeline configuration

Mesh generation is crucial, as poor mesh quality can lead to grid distortion and computational interruptions. ICEM is used to mesh the pipeline and divide it into hexahedral elements. ICEM is a tool for meshing with the model in ANSYS software. To ensure that material properties and fluid flow are effectively transferred during model calculation, common mesh nodes must be maintained. A boundary layer was added near the pipeline wall to refine the mesh and improve slurry flow prediction. The grid structure is shown in Figure 3.

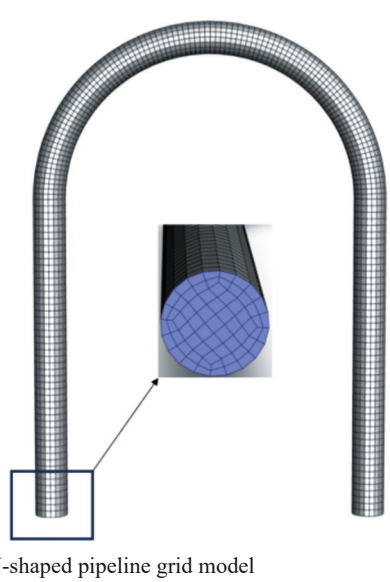


Figure 3 U-shaped pipeline grid model

3.2 Boundary conditions and time step

The speed inlet is set at one end of the pipeline, and a free outlet exists at the other end. The Hertz–Mindlin no-slip contact model is used for interparticle interactions, whereas the Hertz–Mindlin integrated with the Oka wear model is used for interactions between particles and the wall. The Euler–Lagrange two-way coupling method is employed to separately track the motion of the continuous and discrete phases. A particle generator with a diameter equal to that of the pipeline is established (Levy and Chik, 1983), and particle generation positions are randomly distributed. During calculations, the interaction between particles and the fluid, as well as the particle volume fraction, must be considered. The Di Felice drag model is used to calculate the drag force between particles and the fluid, while the Saffman lift, Magnus, and fluid-induced torque are used as lift models in the simulation. According to the relevant data of deep-sea mining transport pipelines, the parameters for pipeline materials and particle materials are shown in Table 1, and the interaction coefficients between particles and between particles and pipeline are shown in Table 2.

Table 1 Basic material parameters

Parameter	Value
Pipe diameter (mm)	200
Pipe material	Nylon
Pipe density (kg/m^3)	1020
Pipe shear modulus (GPa)	1.77
Pipe poisson's ratio	0.393
Continuous phase fluid	Seawater
Fluid density (kg/m^3)	1 123
Fluid viscosity (Pa·s)	0.000 5
Discrete phase particle	Nodules
Particle density (kg/m^3)	3 650
Particle Poisson's ratio	0.25
Gravitational acceleration (m/s^2)	−9.81

Table 2 Contact parameters for materials

Interaction	Restitution coefficient	Static friction coefficient	Rolling friction coefficient
Particle–particle	0.6	0.308	0.30
Particle–pipeline	0.7	0.500	0.01

Pipeline walls are treated as no-slip walls, and the Realizable $k-\varepsilon$ turbulence model is used under transient conditions with a turbulence intensity of 5%. The couple solver is employed for pressure–velocity coupling calculations to improve computational speed and avoid singularities in the pressure and velocity fields, ensuring that the results

quickly converge and stabilize.

In the coupling process, the time step of the particle phase is limited by the Rayleigh time step Δt_p, which is calculated using the following formula:

$$\Delta t_p = \frac{\pi D_p}{0.163\,1\mu_p + 0.876\,6}\sqrt{\frac{2\rho_p\left(1+\mu_p\right)}{E_p}} \tag{8}$$

The Poisson's ratio and Young's modulus of the particles are denoted by μ_p and E_p, respectively. Variations in particle parameters under different operating conditions can lead to changes in the Rayleigh time step. According to the simulation validation results of Tsuji et al. (1993), the fluid time step can be 10–100 times larger than the solid particle time step.

4 Orthogonal experimental analysis of multiple influencing factors

The orthogonal experimental method is an efficient and scientific approach for experimental design and analysis, which can systematically explore the effects of various factors on experimental outcomes. Deep-sea mining pipelines operate in a complex and multi-factor erosive environment. Through orthogonal experimental analyses, the sensitivity of different influencing factors to the maximum erosion rate can be determined, along with the optimal operating conditions for deep-sea mining pipelines.

4.1 Orthogonal experiment factors and design

Parameters such as the bend radius, slurry velocity, mineral particle size, volume fraction, and shear modulus are considered as factors, each factor set at four levels, as presented in Table 3.

Table 3 Orthogonal experimental factors and levels for the deep-sea mining pipeline

Level	A (Bend radius) (m)	B (Slurry velocity) (m/s)	C (Mineral particle size) (mm)	D (Volume fraction) (%)	E (Shear modulus) (GPa)
1	1	2.5	8	5	30
2	2	3	14	10	50
3	2.5	3.5	20	15	70
4	3	4.5	26	20	80

Based on the number of parameters and levels in the factor-level table, an L_{16} (4^5) orthogonal experimental design was developed. By varying the factor levels of different parameters, the variation pattern of the maximum erosion rate in deep-sea mining was investigated, as shown in Table 4.

Table 4 Orthogonal experimental design for the deep-sea mining pipeline

Experiment No.	Level				
	A	B	C	D	E
1	1	1	1	1	1
2	1	2	2	2	2
3	1	3	3	3	3
4	1	4	4	4	4
5	2	1	2	3	2
6	2	2	1	4	3
7	2	3	4	1	4
8	2	4	3	2	1
9	3	1	3	4	2
10	3	2	4	3	1
11	3	3	1	2	4
12	3	4	2	1	3
13	4	1	4	2	3
14	4	2	3	1	4
15	4	3	2	4	1
16	4	4	1	3	2

4.2 Results analysis

Numerical simulations were conducted according to the orthogonal experimental design, and the statistical results were obtained using the maximum erosion rate as the experimental indicator, as shown in Table 5. Analysis of these results determines the influence of different parameter levels on the erosion of deep-sea mining pipelines, enabling the identification of decisive parameters and the optimal combination of parameter levels to minimize erosion.

Here, k_i represents the arithmetic mean of the maximum erosion rates corresponding to level i (i = 1, 2, 3, and 4) for any given column. The difference between the maximum value (k_{max}) and the minimum value (k_{min}) for the same parameter is defined as the range (Yang et al., 2022). A larger range indicates a greater influence of the parameter's variation within the experimental range on the maximum erosion rate. Without considering interactions between parameters, the range values in Table 5 indicate the order of influence of the five factors on the erosion rate of deep-sea mining pipelines as follows: B (slurry velocity) > C (mineral particle size) > D (volume fraction) > E (shear modulus) > A (bend radius).

To intuitively reflect the influence patterns and trends of different factors on pipeline erosion, a trend chart of factor indices was plotted. The horizontal axis represents the four levels of each factor, whereas the vertical axis represents

Table 5 Numerical simulation results of orthogonal experiments

Experiment design	Level					Maximum erosion rate (μm/h)
	Bend radius (m)	Slurry velocity (m/s)	mineral particle size (mm)	Volume fraction (%)	Shear modulus (GPa)	
$A_1B_1C_1D_1E_1$	1	2.5	8	5	30	210.294
$A_1B_2C_2D_2E_2$	1	3	14	10	50	133.541
$A_1B_3C_3D_3E_3$	1	3.5	20	15	70	55.500
$A_1B_4C_4D_4E_4$	1	4.5	26	20	80	69.978
$A_2B_1C_2D_3E_2$	2	2.5	14	15	50	34.920
$A_2B_2C_1D_4E_3$	2	3	8	20	70	240.300
$A_2B_3C_4D_1E_4$	2	3.5	26	5	80	135.000
$A_2B_4C_3D_2E_1$	2	4.5	20	10	30	423.300
$A_3B_1C_3D_4E_2$	2.5	2.5	20	20	50	125.190
$A_3B_2C_4D_3E_1$	2.5	3	26	15	30	164.070
$A_3B_3C_1D_2E_4$	2.5	3.5	8	10	80	1053.900
$A_3B_4C_2D_1E_3$	2.5	4.5	14	5	70	1200.600
$A_4B_1C_4D_2E_3$	3	2.5	26	10	70	10.890
$A_4B_2C_3D_1E_4$	3	3	20	5	80	64.890
$A_4B_3C_2D_4E_1$	3	3.5	14	20	30	225.833
$A_4B_4C_1D_3E_2$	3	4.5	8	15	50	807.873
k_1	117.3282	95.3235	578.0917	402.6960	255.8741	–
k_2	73.4847	150.7002	398.7233	405.4077	275.3809	–
k_3	100.1745	367.5581	167.2200	265.5907	376.8225	–
k_4	120.0495	625.4377	94.9845	165.3251	330.9420	–
R	46.5648	530.1142	483.1072	240.0826	120.9484	–

the corresponding k_i (i = 1, 2, 3, and 4) values of the experimental indicators. This trend chart visually illustrates how the experimental indicators vary with different parameter levels and their interactions with other parameters.

Figure 4 shows that when Factor A (Bend Radius) increases, the erosion rate of the deep-sea mining pipeline first decreases and then increases. When the bend radius is small, the fluid is easily obstructed, forming turbulence that results in a high erosion rate. As the bend radius increases, the slurry flows more smoothly, reducing the erosion rate. However, with a significant increase in the bend radius, minerals tend to remain longer at the bend, causing the erosion rate to rise. Figure 5 shows that as the slurry velocity increases, the erosion rate increases monotonically. At low velocities, the kinetic energy of the minerals is low, resulting in a lower erosion rate. As the velocity increases, the kinetic energy of the minerals also increases, causing a significant rise in erosion. Figure 6 indicates that as the mineral particle size increases, the erosion rate decreases. When the particle size is small, the kinetic energy is high; as the particle size increases, the gravitational influence on the mineral particles reduces their kinetic energy. Figure 7 shows that as the volume fraction increases, the erosion rate first rises gradually and then decreases sharply. With increasing volume fraction, the number of particles per unit volume increases significantly, leading to more frequent collisions between particles and the pipe wall, which aggravates erosion. However, when the particle volume fraction becomes too high, particles are more likely to collide with each other and cause blockages, resulting in a reduced erosion rate. Figure 8 shows that the shear modulus is positively correlated with the pipeline erosion rate. As particle hardness increases, the erosion amount also increases. However, when the shear modulus reaches 80 GPa, the erosion rate decreases, as this trend is also influenced by other parameters.

4.3 Optimization scheme

For deep-sea mining pipelines, minimizing the maximum erosion rate is the primary objective. Based on the range analysis in Table 5 and the trend charts in Figures 4–8, it can be concluded that the optimal conditions occur when the bend radius is 1 m, the slurry velocity is 2.5 m/s, the mineral particle size is 26 mm, the volume fraction is 20%, and the shear modulus is 30 GPa. Under these conditions, the maximum erosion rate is minimized, corresponding to the optimal parameter combination $A_2B_1C_4D_4E_1$. To

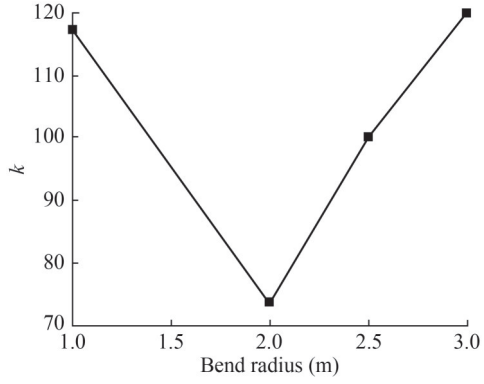


Figure 4 Influence of different bend radii on k

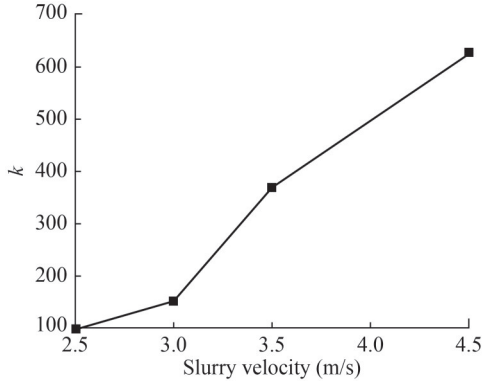


Figure 5 Influence of different slurry velocities on k

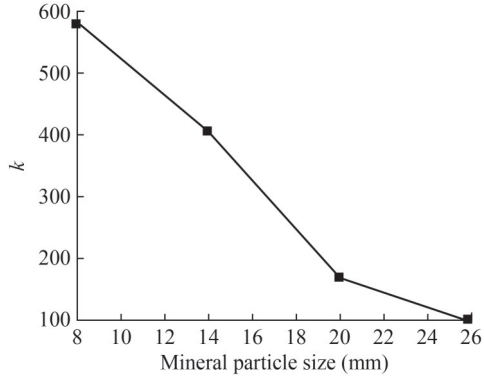


Figure 6 Influence of different mineral particle sizes on k

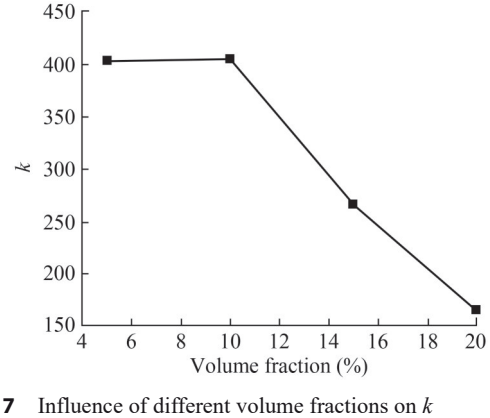


Figure 7 Influence of different volume fractions on k

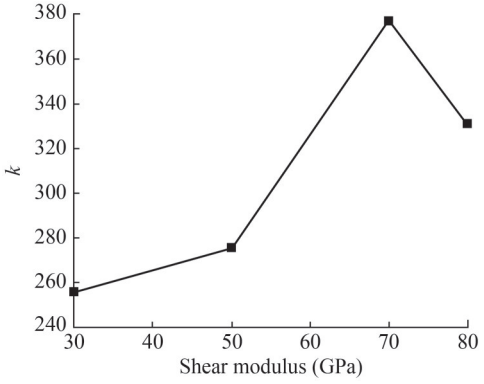
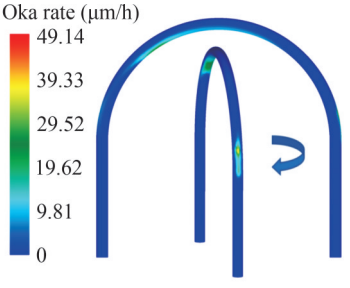
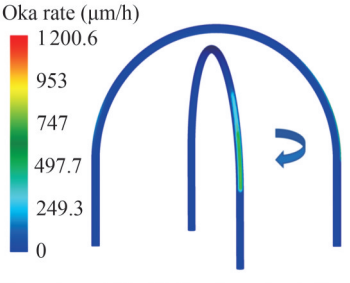


Figure 8 Influence of different shear moduli on k

demonstrate that the optimal conditions significantly reduce the erosion rate of the deep-sea mining pipeline, a comparison of the cloud diagram between the optimal conditions and Experiment No. 12 ($A_3B_4C_2D_1E_3$), which has the highest values in the experiment, is shown in Figure 9.



(a) Erosion cloud diagram of the optimal condition experiment



(b) Experiment No.12 Erosion cloud diagram

Figure 9 Erosion rate distribution

Figure 9 shows that the maximum erosion rate under the optimal condition experiment is significantly reduced, compared to Experiment No. 12, decreasing by approximately two orders of magnitude. Additionally, the erosion range is notably smaller. These results demonstrate that the optimal condition can play a crucial role in enhancing the efficiency and sustainability of deep-sea mining operations.

5 Single-factor influence experiment analysis

Compared with orthogonal experimental analysis, single-factor experimental analysis can more clearly deter-

mine the causal relationship between a specific factor and the observed result, which is helpful for gaining a deeper understanding of the intrinsic laws of the phenomenon. A U-shaped pipe with a bend radius of 2 m was selected to design a single-factor influence experiment, where the effects of different slurry velocities, mineral particle sizes, volume fractions, and shear modulus values on the solid–liquid two-phase flow in the U-shaped pipe were investigated.

5.1 Single-factor experiment design

By setting four levels for each influencing factor, 16 single-factor experimental schemes were designed, as shown in Table 6.

Table 6 Single-factor experimental parameters

Experiment group	Slurry velocity (m/s)	Mineral particle size (mm)	Volume fraction (%)	Shear modulus (GPa)
1	2.5	14	10	30
2	3	14	10	30
3	3.5	14	10	30
4	4.5	14	10	30
5	3	8	10	30
6	3	14	10	30
7	3	20	10	30
8	3	26	10	30
9	3	14	5	30
10	3	14	10	30
11	3	14	15	30
12	3	14	20	30
13	3	14	10	30
14	3	14	10	50
15	3	14	10	70
16	3	14	10	80

5.2 Influence of the slurry velocity

At a mineral particle size of 14 mm, a volume fraction of 10%, and a shear modulus of 30 GPa, the effects of slurry velocities of 2.5, 3, 3.5, and 4.5 m/s on the erosion wear regions and the maximum erosion rate of the U-shaped pipeline were analyzed.

Figure 10 shows that erosion wear in the U-shaped pipe mainly occurs in two regions: the outer surfaces of the left and right bend segments. This is because, after the fluid-carrying particles exit the first bend segment, they are subjected to the combined effects of gravity, centrifugal force, and secondary flow, causing significant collisions with the outer convex side wall. Consequently, pronounced erosion marks form on the outer region of the second bend segment. Figure 11 shows that the maximum erosion rate of the U-shaped pipe is directly proportional to the slurry velocity. At increased flow velocities, the kinetic energy of the particles increases significantly, leading to increased collision energy and accelerated shedding of pipe wall materials. At a slurry velocity of 4.5 m/s, the maximum erosion rate reaches 487.69 μm/h, which is 350.8 μm/h higher than that at 2.5 m/s.

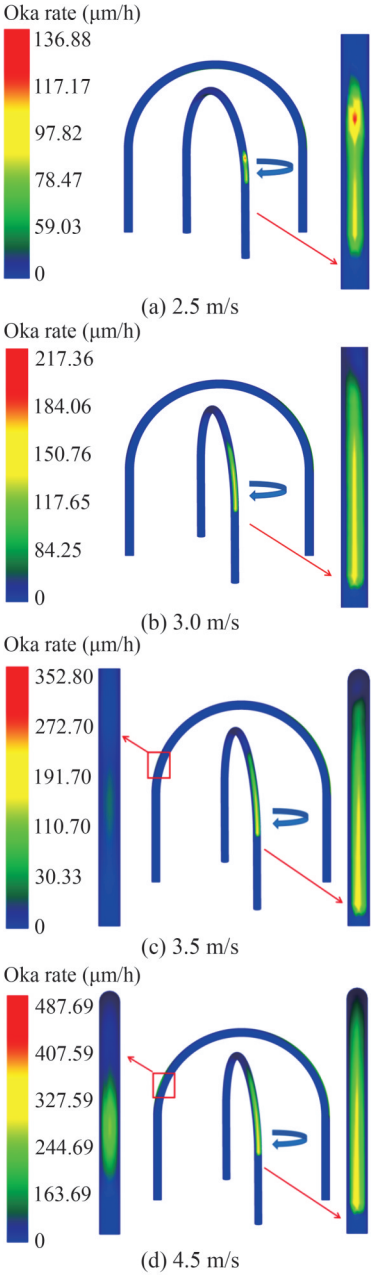


Figure 10 Erosion regions of the U-shaped pipe at different slurry velocities

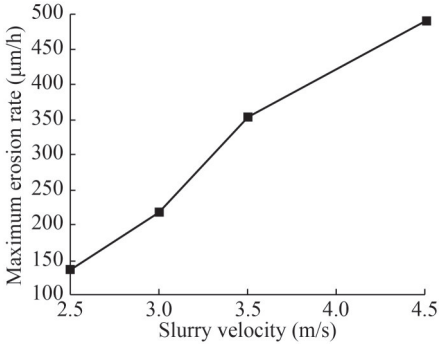


Figure 11 Maximum erosion rate of the U-shaped pipe at different slurry velocities

5.3 Influence of mineral particle size

At a slurry velocity of 3 m/s, volume fraction of 10%, and shear modulus of 30 GPa, the effects of mineral particle sizes of 8, 14, 20, and 26 mm on the erosion wear regions and the maximum erosion rate of the U-shaped pipeline were analyzed.

The erosion of the pipeline is shown in Figure 12. For different mineral particle sizes, erosion wear on the U-shaped pipe mainly occurs in two areas: the outer surfaces of the left and right bend segments. As the particle size increases, the erosion wear region on the outer surface of the bend gradually enlarges, from being concentrated along a single line to eventually covering the entire outer wall surface. From Figure 13 shows that as the mineral particle size increases, the maximum erosion rate of the deep-sea mining pipeline shows a decreasing trend. This is mainly because, as the particle mass increases, the inertia of particles increases, and the particles are less likely to follow the fluid flow, which in turn reduces the kinetic energy of the particles, resulting in a weakened erosion effect on the wall of deep-sea pipelines. Additionally, larger particles have greater contact areas with the pipe wall, resulting in a lower impact force per unit area. Furthermore, as particle size increases, the number of particles within the pipe decreases, leading to fewer collisions, ultimately reducing the maximum erosion rate of the pipeline.

5.4 Influence of volume fraction

At a slurry velocity of 3 m/s, mineral particle size of 14 mm, and shear modulus of 30 GPa, the effects of volume fractions of 5%, 10%, 15%, and 20% on the erosion wear regions and the maximum erosion rate of the U-shaped pipeline were analyzed.

The erosion of the pipeline is shown in Figure 14. At different volume fractions, erosion wear on the U-shaped pipe remains primarily concentrated on the outer sides of the right and left bend segments. As the volume fraction increases, noticeable changes occur in the erosion regions and the most severely eroded areas of the U-shaped pipe,

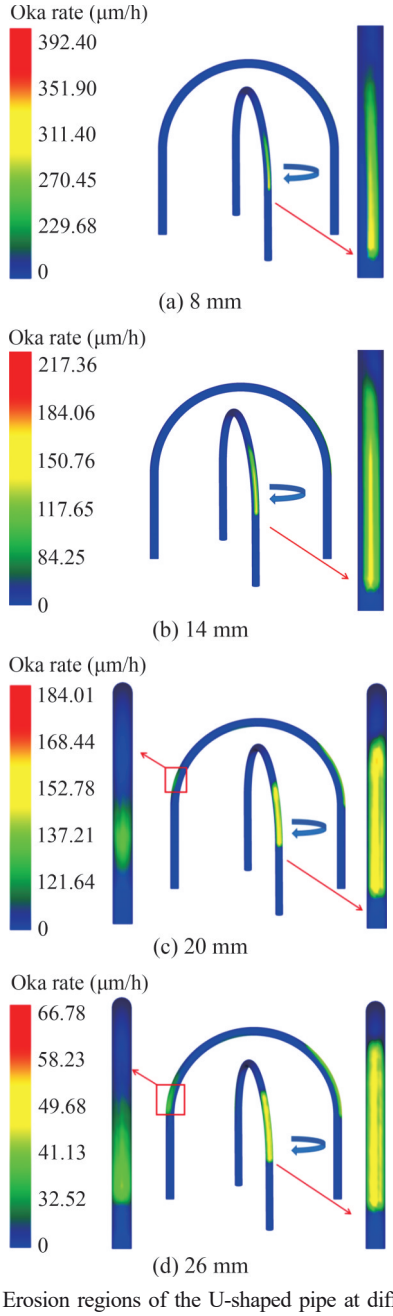


Figure 12 Erosion regions of the U-shaped pipe at different mineral particle sizes

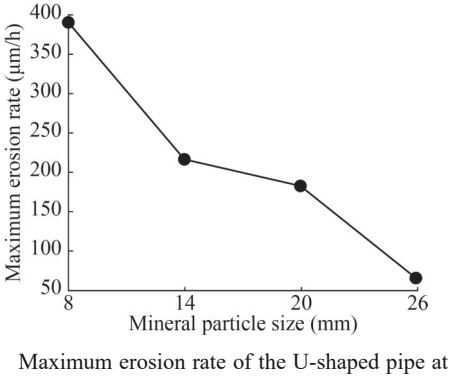


Figure 13 Maximum erosion rate of the U-shaped pipe at different mineral particle sizes

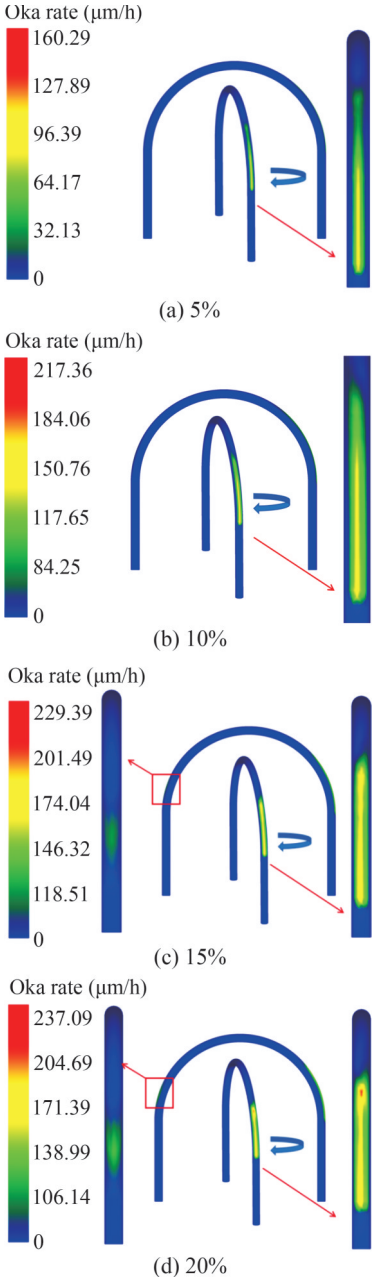


Figure 14 Erosion regions of the U-shaped pipe at different volume fractions

with the maximum erosion rate appearing on the outer side of the right bend segment. Figure 15 shows that the erosion rate is positively correlated with the volume fraction. As the volume fraction increases, the number of particles in the pipeline increases, enhancing the collision frequency between particles and the pipe wall. This rise in particle concentration intensifies collisions with the pipe wall, aggravating erosion on the outer side of the right bend segment. However, after reaching a certain value, collisions between particles can reduce the kinetic energy of individual particles to some extent, which explains why the rate of erosion increase slows as the volume fraction rises. For example, as the volume fraction increases from 5% to 10%, the erosion rate increases by 57 μm/h, whereas from 10% to 20%, the average increase is only 9.9 μm/h.

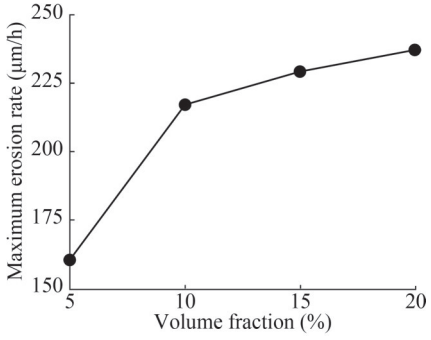


Figure 15 Maximum erosion rate of the U-shaped pipe at different volume fractions

5.5 Influence of the shear modulus

At a slurry velocity of 3 m/s, mineral particle size of 14 mm, and a volume fraction of 10%, the effects of shear moduli of 30, 50, 70, and 80 GPa on the erosion wear regions and the maximum erosion rate of the U-shaped pipeline were analyzed.

The erosion patterns of the pipeline are illustrated in Figure 16. Across different shear modulus values, erosion remains predominantly concentrated on the outer sides of the right and left bend segments. As the shear modulus increases, the overall erosion region and the area experiencing the most severe erosion undergo significant changes. Figure 17 shows that the maximum erosion rate of the U-shaped pipe initially decreases, then increases, and finally decreases again as the shear modulus rises. At 30 GPa, particle–pipe interactions are relatively weak, resulting in low erodibility. At 50 GPa, most collisions are elastic. At 70 GPa, the particle edges are more likely to cut into the pipe material, increasing the erosion rate. Further increases in the shear modulus result in increased hardness and brittleness of the particles, causing them to fracture more easily upon impact, thereby reducing the erosion rate.

5.6 Experimental comparative analysis

As shown in Table 7, differences between the maximum and minimum erosion rates across experimental groups were compared. This helps determine the factor variation that most significantly affects erosion in deep-sea mining pipelines.

Table 7 presents the influence of variations in different factors on the erosion of deep-sea mining pipelines in descending order as follows: mud flow velocity > mineral particle size > volume fraction > shear modulus. This result is consistent with that of the orthogonal experiment, suggesting that mud flow velocity is a critical variable affecting the erosion of deep-sea mining pipelines.

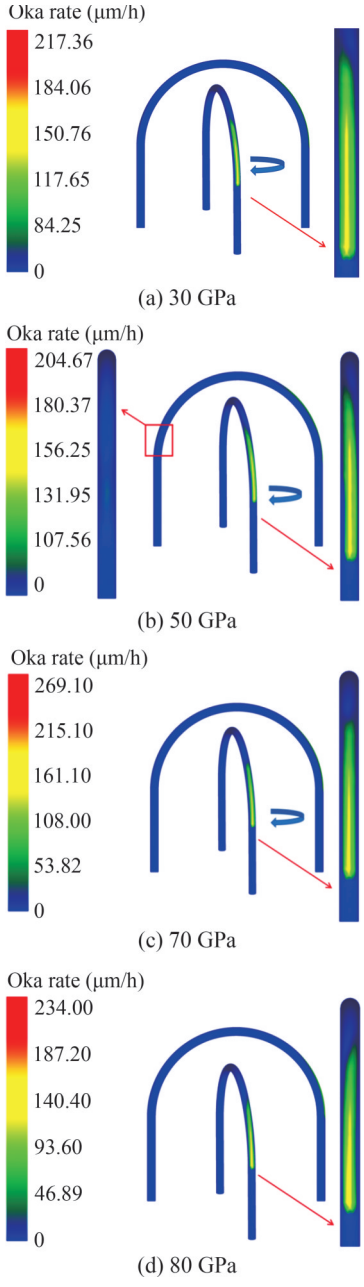


Figure 16 Erosion regions of the U-shaped pipe at different shear moduli

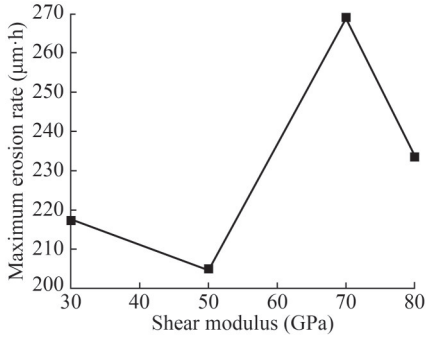


Figure 17 Maximum erosion rate of the U-shaped pipe at different shear moduli

Table 7 Comparison of erosion rate differences under different influencing factors of pipelines

Factors	Mud flow velocity		Mineral particle size		Volume fraction		Shear modulus	
Erosion rate (μm/h)	Min	Max	Min	Max	Min	Max	Min	Max
	136.88	487.68	66.78	392.4	160.29	237.09	204.67	269.1
Difference (μm/h)	350.8		325.62		76.8		64.43	

6 Conclusions

This study comprehensively investigated the erosion mechanisms of deep-sea mining pipelines. The key findings of this study are summarized as follows:

1) For mineral particles with diameters in the range of 5–30 mm, the "Gaussian Volume Distribution Method" was employed to replace the "Sampling Point Method", thereby refining the volume fraction algorithm for mineral particles. This improved algorithm enables the correction of particle volume fraction, enhancing the accuracy of calculations for volume fraction, flow field, and drag force.

2) Orthogonal experimental analysis revealed the relative influence of five factors on the erosion rate of deep-sea mining pipelines, ranked as follows: B (Slurry Velocity) > C (Mineral Particle Size) > D (Volume Fraction) > E (Shear Modulus) > A (Bend Radius), based on the range R values.

3) The trend chart of indices indicates that the threshold maximum erosion rate is achieved under the following optimal parameter combination: $A_2B_1C_4D_4E_1$, corresponding to a bend radius of 1 m, slurry velocity of 2.5 m/s, mineral particle size of 26 mm, volume fraction of 20%, and shear modulus of 30 GPa. A comparison between the optimal condition experiment and Experiment No. 12 ($A_3B_4C_2D_1E_3$) showed a significant difference of 1 151.46 μm/h in erosion rates. These findings can be applied to significantly reduce the erosion risk of deep-sea mining pipelines and are of great significance for ensuring the long-term stable operation of the pipelines.

4) Single-factor experimental analysis identified the primary erosion wear locations and their severity on the U-shaped pipe, ordered as follows: the outer side of the outlet bend, the outer side of the inlet bend, and the inner side of the semicircular bend. Results revealed that the inlet velocity and volume fraction were directly proportional to the maximum erosion rate of the U-shaped pipe, whereas mineral particle size exhibited an inverse relationship. The shear modulus demonstrated a trend of initial decrease, followed by an increase, and then another decrease. These findings clarify the erosion characteristics of deep-sea mining pipelines, provide a scientific basis for the optimized

design of pipeline structures and the selection of key protection areas, and are of great significance for extending the service life of the pipelines.

5) In the single-factor experimental analysis, at a velocity of 4.5 m/s, the maximum erosion rate of the pipeline reached 487.69 μm/h, representing an increase of 350.8 μm/h, compared to the rate at 2.5 m/s. When the particle size was 8 mm, the maximum erosion rate was 392.4 μm/h, which was 325.62 μm/h higher than that observed for a particle size of 26 mm. When the volume fraction exceeded 10%, the rate of increase in the maximum erosion rate diminished, with the average increase in the maximum erosion rate between 10% and 20% volume fraction being 9.9 μm/h. At a shear modulus of 70 GPa, the maximum erosion rate of the pipeline was 269.1 μm/h, which was 64.43 μm/h higher than that at a shear modulus of 50 GPa.

Funding Supported by Jiangsu Province's Frontier Technology R & D Program (BF2025015), the China State Shipbuilding Corporation Limited Special Project (Grant No. 202205Z) and the National Key Research and Development Program of China (Grant No. 2021YFC 2801600).

Competing interests The authors have no competing interests to declare that are relevant to the content of this article.

References

Agrawal M, Khanna S, Kopliku A, Lockett T (2019) Prediction of sand erosion in CFD with dynamically deforming pipe geometry and implementing proper treatment of turbulence dispersion in particle tracking. Wear 426: 596-604. DOI: 10.1016/j. wear. 2019. 01.018

Cai Q, Ma W, Rao Q, Li G (2020) Optimization design of bionic grousers for the crawled mineral collector based on the deep-sea sediment. Marine Georesources & Geotechnology 38(1): 48-56. DOI: 10.1080/1064119x.2018.1551446

Chen W, Xu HL, Wu B, Yang FQ, Lin P, Hu D (2022) Spatial configuration and static characteristics of hoses in deep-sea ore conveying system. Ocean Engineering 247: 110649. DOI: 10.1016/j. oceaneng.2022.110649

Chen W, Zhang P, Sun Y, Wu Y, Zheng C, Xu H, Li Z (2022) Numerical simulation of hydraulic transport of non-spherical particles based on CFD-DEM. China Powder Science and Technology 28(5): 82-91. DOI: 10.13732/j. issn. 1008-5548.2022. 05.011

Helgaker JF, IJzermans S, Landheim TJ, Eeg TB, Hverven SM, Piotrowski P (2017) Large-scale erosion testing of an unbonded flexible pipe. SPE Journal 22(3): 736-745. DOI: 10.2118/181761-pa

Kannojiya V, Deshwal M, Deshwal D (2018) Numerical analysis of solid particle erosion in pipe elbow. Materials Today: Proceedings 5(2): 5021-5030. DOI: 10.1016/j.matpr.2017.12.080

Kannojiya V, Kumar S, Kanwar M, Mohapatra SK (2016) Simulation of erosion wear in slurry pipe line using CFD. Applied Mechanics and Materials 852: 459-465. DOI: 10.4028/www. scientific. net/ amm.852.459

Kleis I, Kulu P (2007) Solid particle erosion: Occurrence, prediction and control. Springer, London. https://doi.org/10.1007/978-1-84800-029-2

Lain S, Sommerfeld M (2019) Numerical prediction of particle erosion of pipe bends. Advanced Powder Technology 30(2): 366-383. DOI: 10.1016/j.apt.2018.11.014

Levy AV, Chik P (1983) The effects of erodent composition and shape on the erosion of steel. Wear 89(2): 151-162. DOI: 10.1016/ 0043-1648(83)90240-5

Liu G, Wang M, Xu L, Incecik A, Sotelo MA, Li Z, Li W (2020) A new bionic lateral line system applied to pitch motion parameters perception for autonomous underwater vehicles. Applied Ocean Research 99: 102142. DOI: 10.1016/j.apor.2020.102142

Liu L, Zhang X, Tian X, Li X (2023) Numerical investigation on dynamic performance of vertical hydraulic transport in deep-sea mining. Applied Ocean Research 130: 103443. DOI: 10.1016/j. apor.2022.103443

Loth E, Dorgan AJ (2009) An equation of motion for particles of finite Reynolds number and size. Environmental Fluid Mechanics 9: 187-206. DOI: 10.1115/fedsm2009-78212

Oka YI, Okamura K, Yoshida T (2005) Practical estimation of erosion damage caused by solid particle impact: Part 1: Effects of impact parameters on a predictive equation. Wear 259(1-6): 95-101. DOI: 10.1016/j.wear.2005.01.040

Parenteau T (2012) Flow assurance for deep ocean mining: Large-scale experiment for flow correlation validation and abrasion testing. Offshore Technology Conference, Houston, USA, OTC-23250-MS. DOI: 10.4043/23250-ms

Peng W, Cao X (2016) Numerical prediction of erosion distributions and solid particle trajectories in elbows for gas-solid flow. Journal of Natural Gas Science and Engineering 30: 455-470. DOI: 10.1016/j.jngse.2016.02.008

Rongau J, Viale S (2017) Development of a flexible pipe for deep sea mining. Offshore Technology Conference, Houston, USA, OTC-27658-MS. DOI: 10.4043/27658-ms

Sande PC, Ray S (2014) Mesh size effect on CFD simulation of gas-fluidized Geldart A particles. Powder Technology 264: 43-53. DOI: 10.1016/j.powtec.2014.05.019

Sommerfeld M (2003) Analysis of collision effects for turbulent gas–particle flow in a horizontal channel: Part I. Particle transport. International Journal of Multiphase Flow 29(4): 675-699. DOI: 10.1016/s0301-9322(03)00031-4

Takano S, Sato H, Terao T, Masanobu S, Kawano S (2022) Study on pipe wear based on large scale experiment and scale effect for deep sea mining. Journal of Offshore Mechanics and Arctic Engineering 144(1): 011803. DOI: 10.1115/1.4052178

Tsuji Y, Kawaguchi T, Tanaka T (1993) Discrete particle simulation of two-dimensional fluidized bed. Powder Technology 77(1): 79-87. DOI: 10.1016/0032-5910(93)85010-7

Wang H, Yu Y, Xu Y, Zhang S, Li X (2022) A simple approach for coarse particle stress-erosion test with experimental validation. Journal of Materials Engineering and Performance 31(7): 5823-5836. DOI: 10.1007/s11665-022-06623-9

Wang K, Li X, Wang Y (2017) Numerical investigation of the erosion behavior in elbows of petroleum pipelines. Powder Technology 314: 490-499. DOI: 10.1016/j.powtec.2016.12.083

Yang X, Guan L, Li Y, Zhang Y, Wang G, Yan D (2022) Numerical simulation and experimental study on erosion-corrosion of square elbow based on orthogonal test. Journal of Chinese Society for Corrosion and protection 42(6): 979-987. DOI: 10.11902/1005.

4537.2021.325

Yu J, Li H, Yu Y, Liu X, Xu W, Wang H, Liu P (2022) Numerical investigation of liquid-solid erosion in unbonded flexible pipes. International Journal of Pressure Vessels and Piping 199: 104743. DOI: 10.1016/j.ijpvp.2022.104743

Zahari NM, Zawawi MH, Sidek LM, Mohamad D, Itam Z, Ramli MZ, Syamsir A, Abas A, Rashid M (2018) Introduction of discrete phase model (DPM) in fluid flow: A review. AIP Conference Proceedings 2030(1): 020234. DOI: 10.1063/1.5066875

Zhang R, Liu H, Dong S (2019) Approximate theoretical solution of the movement and erosion of solid particles in a 90-degree bend. Wear 430: 233-244. DOI: 10.1016/j.wear.2019.05.013